Spherical self-consistent atomic deformation model for first-principles energy calculations in ionic crystalline solids

Harold T. Stokes,* L. L. Boyer, and M. J. Mehl
Complex Systems Theory Branch, Naval Research Laboratory, Washington, D.C. 20375
(Received 24 January 1996; revised manuscript received 7 May 1996)

We present a first-principles method [called spherical self-consistent atomic deformation (SSCAD)] for calculating the energy per unit cell in ionic crystalline solids. SSCAD is a density-functional method using the local-density approximation (LDA). Wave functions are localized about each ion, resulting in a single-particle Schrödinger's equation for each ion. To simplify the calculation, we spherically average the potential energy in each of these equations. The electron density is determined from the self-consistent solution of these equations. SSCAD scales as order N and runs very fast, even for crystals with large unit cells. We discuss some of the limitations of SSCAD, and we give examples of using SSCAD to determine crystalline structure, phonon dispersion, elastic moduli, and charge transfer. [S0163-1829(96)07635-7]

I. INTRODUCTION

A major goal of first-principles calculations in solids is to be able to accurately and quickly calculate the structure and properties of a material given only its chemical composition. Such calculations would be invaluable in the design of new materials. Unfortunately, it is a difficult goal to achieve. Generally, accurate calculations are not quick, and quick calculations are not accurate. Appropriate compromises must be found. Fortunately, in some types of materials, we can make simplifying approximations which allow quick, efficient calculations without sacrificing much accuracy.

An example of this is crystalline solids containing closed-shell ions. Gordon and Kim[1] (GK) formulated an electron-gas model for calculating the interaction energy in such solids. They assume the electron density to be a sum of densities localized about each ion. They obtain the electron density about each ion from Hartree-Fock wave functions of the free ion and consider it to be unaffected by the interaction with neighboring ions. The interaction energy is calculated using the local-density approximation (LDA). This simple model produces surprisingly good results in ionic solids.

A number of improvements to the GK method have been implemented over the years (see Gordon and LeSar[2] for an excellent review). One of the shortcomings in the GK method is the use of free-ion electron densities. The crystalline environment affects these densities. Muhlhausen and Gordon[3] approximated the crystalline environment of an ion with a spherical shell of charge (called a Watson sphere[4]) centered at the ion. The charge on the sphere is chosen to be equal in magnitude but opposite in sign to the charge of the ion. The radius of the sphere is chosen so that the potential inside the sphere is equal to the long-range Madelung potential of the crystal at the nucleus of the ion. The electron density of each ion is obtained from wave functions calculated in the presence of the Watson sphere. Using these electron densities, the interaction energy is calculated the same way as in GK, but the intra-ionic energy must now also be included. This approach was also independently developed by Boyer and co-workers[5–7] and was called the potential induced breathing model (PIB).

In PIB, the crystalline environment used for obtaining electron densities of the ions includes only the long-range component of the interactions between ions. Self-consistent methods in which the short-range interactions between ions is also included in the crystalline environment have been implemented by Edwardson[8] and Cortona.[9,10] This type of method was also independently developed by Boyer and co-workers[11–13] and was called the self-consistent PIB model (SCPIB). The total energy of the crystal is written as a functional of the electron density of each of the ions. Using an approach analogous to Kohn and Sham,[14] a single-particle Schrödinger-like equation is obtained for the wave functions of each ion. (We call this the ''Kohn-Sham-like'' or KSL equation.) The solution of that equation results in an electron density for that ion which minimizes the total energy of the crystal with respect to the electron density function for that ion. This is repeated for each ion, one at a time, thus minimizing the energy with respect to the total electron density function in the crystal. The potential in the KSL equation for each ion depends on the electron density function of every ion, and thus the density functions must be determined self-consistently by iteration. More recently, this model has been called the self-consistent atomic deformation model (SCAD). Thus far, this model has only been implemented for the case where the electron densities are constrained to be spherically symmetric about each ion (the spherical SCAD model, or SSCAD).

Recently[15] SSCAD was successfully used in the first-principles calculation of the solubility limits of $Mg_xCa_{1-x}O$. The results agreed quite well with experimental data.

Note that atomic units are used throughout this paper: $\hbar = e = m = 1$, where e and m are the magnitude of the charge and the mass of the electron, respectively. Units of distance are bohr, and units of energy are hartree.

II. METHOD

We assume that electron densities are localized about each ion and that the total electron density is simply the sum of the ionic densities:

$$\rho(\mathbf{r}) = \sum_i \rho_i(r_i), \tag{1}$$

where r_i is the distance from $\mathbf{r}$ to the nucleus of the ith ion and $\rho_i(r_i)$ is the electron density localized at the ith ion and is spherically symmetric about the nucleus of that ion. The total energy of the crystal is written as a functional of the density and is the sum of the kinetic energy, the electrostatic energy, and the exchange-correlation energy.

We use LDA for the exchange-correlation energy,

$$E_{\rm xc} = \int d^3r \rho \epsilon_{\rm xc}(\rho), \tag{2}$$

where $\epsilon_{\rm xc}(\rho)$ is the exchange-correlation energy per electron in a gas of interacting electrons with uniform density ρ. We use the expression of Hedin and Lundqvist[16] for $\epsilon_{\rm xc}(\rho)$. We also use LDA for the extra contribution to kinetic energy due to overlap of ionic densities:

$$E_{\rm k} = \int d^3r \left[\rho \epsilon_{\rm k}(\rho) - \sum_i \rho_i \epsilon_{\rm k}(\rho_i) \right], \tag{3}$$

where $\epsilon_{\rm k}(\rho) = \frac{3}{10}(3\pi^2\rho)^{2/3}$ is the Fermi-Thomas energy, i.e., the kinetic energy per electron in a gas of interacting electrons with uniform density ρ. The energies in Eqs. (2) and (3) arise from many-body interactions, i.e., the expressions cannot be separated into terms that involve only pairs of ions. We can greatly increase the efficiency of SSCAD by using the ''pair approximation,'' as in GK, where the many-body interactions are approximated by interactions between pairs of ions. As we will see, however, this approximation can lead to poor results when considering the transfer of charge between ions.

Writing the total energy as a functional of the electron density, we obtain from density-functional theory a result analogous to that of Kohn and Sham.[14] We obtain for each ion a one-particle Schrödinger-like equation (the KSL equation),

$$-\tfrac{1}{2}\nabla^2\psi(\mathbf{r}) + \overline{V_i}(r_i)\psi(\mathbf{r}) = E\psi(\mathbf{r}), \tag{4}$$

where $\overline{V_i}(r_i)$ is the KSL potential spherically averaged about the nucleus of the ith ion. Using a spherically symmetric potential, we obtain wave functions of the form,

$$\psi_{inlm}(\mathbf{r}) = R_{inl}(r_i) Y_{lm}(\theta_i, \phi_i), \tag{5}$$

where n,l,m are atomic quantum numbers and $Y_{lm}(\theta_i,\phi_i)$ is the spherical harmonic function. The electron density of the ith ion is given by

$$\rho_i(r_i) = \frac{1}{4\pi}\sum_{nl} N_{inl} R^2_{inl}(r_i), \tag{6}$$

where N_{inl} is the number of electrons in the states labeled by n and l. (These electrons are distributed evenly among the states labeled by different values of m.)

The KSL potential $V_i(r_i)$ for each ion is a function of the total electron density $\rho(\mathbf{r})$ which, in turn, can be calculated only after solving Eq. (4) for each ion. We therefore begin with electron densities of isolated ions and then solve for $\rho(\mathbf{r})$ self-consistently by iteration. For most rapid convergence, we mix the densities calculated in each iteration with the densities used in that iteration. (We generally mix 40% of the new density with 60% of the old density.) We then use these mixed densities to calculate the KSL potentials in the next iteration. Details about the calculation of $\overline{V_i}(r_i)$ are given in the Appendix.

In the PIB model, the interionic contribution to the KSL potential is replaced by the electrostatic potential of the Watson sphere. However, the total energy in PIB is calculated exactly as in SSCAD.

Using a spherically symmetric KSL potential, the solutions to the KSL equation in Eq. (4) have the form of Eq. (5) so that the KSL equation actually becomes an ordinary differential equation for $R_{inl}(r_i)$ (the ''radial Schrödinger equation''). We have implemented two different methods for solving that equation. In the first method, we numerically solve the differential equation [numerical solution (NS) method]. In the second method, we use a set of basis functions, calculate matrix elements of the KSL equation, and then diagonalize the matrix [basis functions (BF) method]. In NS, the solution is exact, whereas in BF, the solution is confined to linear combinations of the basis functions used. On the other hand, the calculations in BF require much less time.

In BF, we use as basis functions the Slater basis-set expansions of the Roothaan-Hartree-Fock atomic wave functions compiled by Clementi and Roetti[17] (He-Xe) and by McLean and McLean[18] (Cs-U). We have found these basis functions to be very flexible. When we solve the KSL equations for the atomic wave functions of ions in a crystal, we obtain nearly identical results using NS and BF. We have not found any case where it made any significant difference using NS or BF.

III. APPLICATIONS

We now briefly discuss some applications of SSCAD, including some comparisons with PIB and GK.

A. Crystalline structure

In Fig. 1, we show the energy per unit cell of MgO as a function of the lattice parameter a. Each data point in the figure was calculated using SSCAD. The solid line is simply drawn through the points to guide the eye. The calculation of each data point required about 12 s on a Hewlett Packard workstation (HP 9000). Each calculation involved 32 iterations to solve for the density self-consistently from the KSL equations (starting with wave functions of neutral atoms). SSCAD is fast and precise. We see very little evidence for any digital noise. Note that these calculations are ''order N,'' i.e., the time required scales approximately linearly with the number of atoms in the unit cell. This allows calculations in crystals with very large unit cells. (Actually, the calculation of the Madelung potential is order N^2, but this part of the calculation is only done once and usually takes only a small fraction of the time required for the total calculation.)

From the position of the minimum energy in the figure, we see that SSCAD predicts the lattice parameter of MgO to be about 7.93 bohr. This is very close to the experimentally determined value (7.97 bohr). This agreement in MgO is

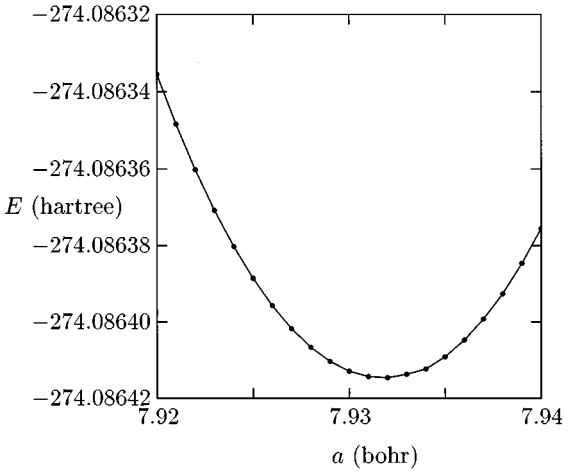

FIG. 1. Energy E per unit cell in MgO as a function of the lattice parameter a. Each data point represents a calculation made with SSCAD.

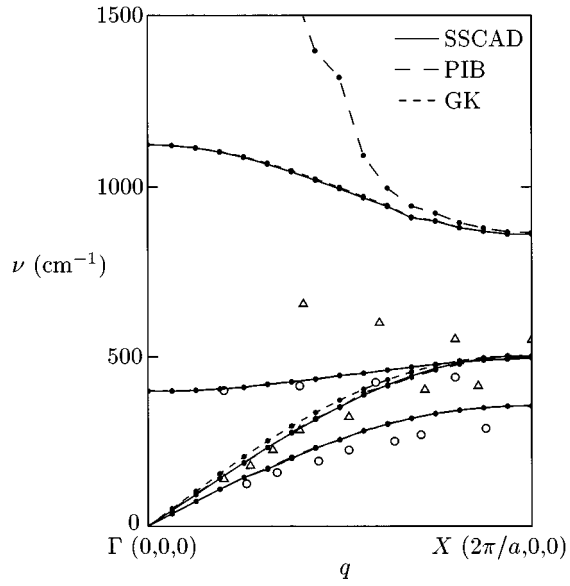

FIG. 2. Phonon spectra calculated for MgO with SSCAD, PIB, and GK (using the ionic densities from SSCAD for the equilibrium structure). Each calculation is plotted as a solid dot. Open circles (transverse modes) and triangles (longitudinal modes) are experimental data from Sangster *et al.* (Ref. 20) (inelastic neutron scattering).

partly accidental, since calculations using LDA are known to usually give results that are too small by about 1–2 %.

We would expect SSCAD to do well in ionic solids, especially when the ions have closed shells, as in MgO. We would also expect SSCAD to not do well when highly covalent bonds are present.

B. Phonon spectra

Phonon spectra can be obtained from first-principles calculations of frozen-phonon energies. The frequencies for the longitudinal optical (LO) branch calculated with PIB diverge as the wave vector approaches zero.[7] This singular behavior can be removed in PIB either by introducing a screening parameter[7] or by minimizing the energy with respect to the Watson sphere radii.[19] SSCAD does not exhibit this problem.[12] Determining densities and potentials self-consistently removes this difficulty.

In Fig. 2, we show the phonon spectra calculated for MgO along the Δ line from Γ to X in the first Brillouin zone. We calculated the frequencies for frozen phonons at 17 equally spaced values of the wave vector q. We used three methods in the calculations: (1) SSCAD, (2) PIB, and (3) GK (using electron densities from SSCAD for the equilibrium structure). In this last method, the electron densities are held rigid. All calculations are plotted as solid dots in the figure.

All three methods give nearly identical results for the transverse branches. The dots and lines for these branches are drawn on top of each other in the figure and cannot be distinguished from each other. In the longitudinal acoustic (LA) branch, SSCAD and PIB give nearly identical results, whereas the GK method gives frequencies which are slightly higher.

In the LO branch, SSCAD and GK give nearly identical results, whereas PIB diverges as q approaches zero. The LO frequency at $q=0$ was determined by adding the amount of frequency enhancement expected for a rigid-ion system with charges 2 and $2-$, in this case 660 cm^{-1}. The LO branch obtained from SSCAD evidently is approaching this value at $q=0$.

The open circles and triangles in the figure show experimental points of Sangster *et al.*,[20] determined by inelastic neutron scattering. We see that the calculations in the LO branch give frequencies which are much too high. The LO enhancement is severely overestimated by the calculations, and SSCAD does not show any improvement over GK. In the other branches, the calculations consistently give frequencies which are 10–20 % too high. Overall, SSCAD does not significantly improve the agreement with experimental data compared to GK.

C. Elastic moduli

The elastic moduli can be calculated from the velocities of sound in a crystal.[21] The velocities can be obtained from the phonon spectra near $q=0$. In MgO, we calculated the velocities of transverse and longitudinal long-wavelength phonons for three different wave vectors: $q=(\pi/8a,0,0)$, $(\pi/8a,\pi/8a,0)$, and $(\pi/16a,\pi/16a,\pi/16a)$. (These correspond to wavelengths between 60 and 100 Å.) This resulted in seven different velocities. In cubic crystals, all velocities can be written in terms of three elastic moduli: C_{11}, C_{12}, and C_{44}. This gives us seven equations and three unknowns. We found the best values of the elastic moduli using a least squares fit. We repeated this calculation using SSCAD, PIB, and GK. For both SSCAD and GK, the fit was excellent. The fit was about ten times worse for PIB.

The results are shown in Table I, along with experimental values from Jackson and Niesler.[22] The agreement with experimental values improves significantly as we move across the table from GK to PIB to SSCAD. Note that GK obeys the Cauchy equality ($C_{12}=C_{44}$ for cubic crystals) as expected for models based on two-body central forces.

We also calculated the elastic moduli using the full Kohn-Sham theory[14] within LDA, by means of the full-potential

TABLE I. Elastic constants in MgO calculated with GK (using the ionic densities from SSCAD for the equilibrium structure), PIB, SSCAD, and LAPW. Experimental values are shown for comparison. Units are GPa.

	GK	PIB	SSCAD	LAPW	Expt.[a]
C_{11}	393	355	318	285	297
C_{12}	198	132	123	84	95
C_{44}	201	195	201	150	156

[a]Experimental data from Jackson and Niesler (Ref. 22).

linearized augmented plane wave (LAPW) method using finite strains.[23] This method applies the Kohn-Sham theory with *no* approximations other than the local-density approximation. The results are shown in the table.

D. Charge transfer

Some materials are best modeled with fractional charges on the ions. As an example, we consider $BaTiO_3$. The charges of the closed-shell ions are Ba^{2+}, Ti^{4+}, and O^{2-}. When we solve the KSL equation (4) in SSCAD (using the experimentally determined lattice parameter $a=7.6$ bohr at room temperature), we find that the KSL energy (the eigenvalues of the KSL equation) is lower for the empty Ti $3d$ orbitals than for the full O $2p$ orbitals. This means that we can lower the total energy of the crystal by transferring some charge from the O to the Ti ions. As we transfer charge, the KSL energy of the Ti $3d$ orbitals increases until the KSL energy of the Ti $3d$ orbitals is equal to that of the O $2p$ orbitals. This happens when the Ti $3d$ orbitals contain about 0.24 electron and the O $2p$ orbitals in each oxygen ion contain about 5.92 electrons. If we transfer additional charge, the KSL energy of the Ti $3d$ orbitals rises above that of the O $2p$ orbitals, now causing the total energy to increase instead of decrease. The KSL energies for these orbitals are shown in Fig. 3. The total energy per unit cell is shown in Fig. 4. The minimum energy occurs exactly at the point where the two levels cross in Fig. 3.

This result is in agreement with Janak's theorem,[24] which Cortona[9] proved to apply to the present case. The jth eigenvalue E_{ij}^{KSL} of the KSL equation for the ith ion is related to the total energy E per unit cell by

$$E_{ij}^{\mathrm{KSL}}=\partial E/\partial N_{ij}\,, \tag{7}$$

where N_{ij} is the number of electrons occupying the orbitals corresponding to that eigenvalue. Applying this equation to Figs. 3 and 4, we obtain

$$E=\int (E_{\mathrm{Ti}\,3d}^{\mathrm{KSL}}-E_{\mathrm{O}\,2p}^{\mathrm{KSL}})\,dQ, \tag{8}$$

where ΔQ is the amount of charge transferred from the O to the Ti ions. The result of this integral, using the data in Fig. 3, is shown as a solid line in Fig. 4. The constant of integration was chosen to match the energy at the minimum. The excellent agreement between the data points calculated directly with SSCAD and the solid line calculated from the KSL energies demonstrates the validity of Janak's theorem in this case.

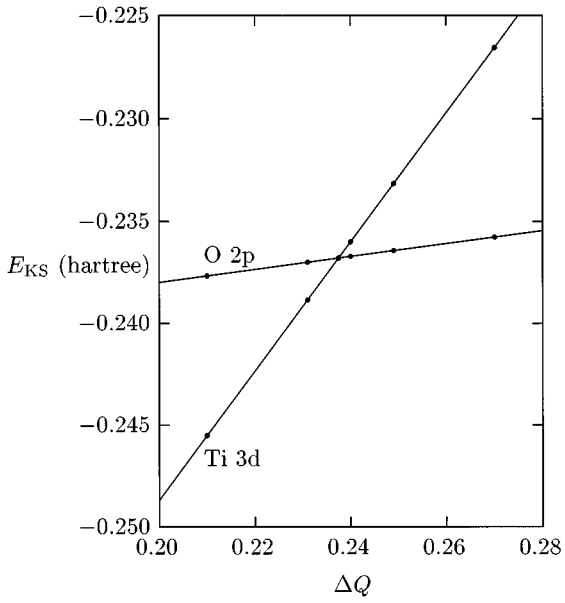

FIG. 3. Kohn-Sham-like energy levels E^{KSL} of the O $2p$ orbitals and the Ti $3d$ orbitals in $BaTiO_3$ as a function of charge transfer ΔQ from the O $2p$ orbitals to the Ti $3d$ orbitals. The data points represent calculations using SSCAD. The lines are simply straight lines drawn through the data points.

Boyer and Mehl[11] made a similar calculation but found that the energy minimum did not occur where the eigenvalues cross. At the time, they thought that this occurred because SSCAD is only approximately variational. Actually, SSCAD is in principle exactly variational.[13] Their results were probably due to approximations in calculating the KSL potential. (1) They used a ''cutoff'' form for the short-range overlap potential, and (2) they calculated the KSL potential

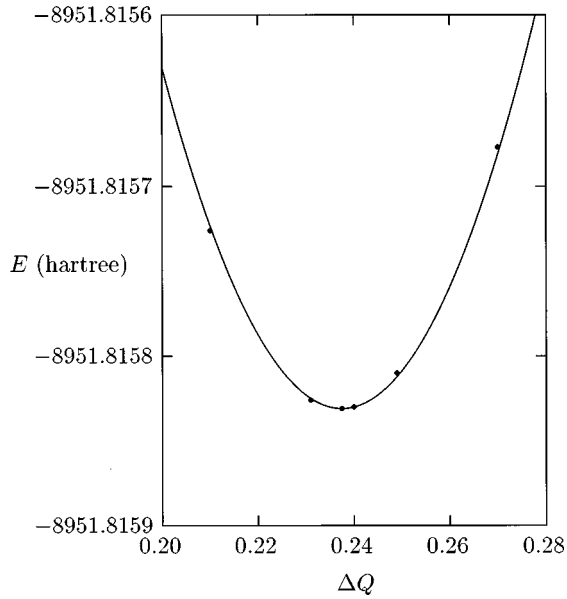

FIG. 4. Total energy E per unit cell of $BaTiO_3$ as a function of charge transfer ΔQ from the O $2p$ orbitals to the Ti $3d$ orbitals. The data points represent calculations using SSCAD. The solid line is obtained from the integration of the difference of the two Kohn-Sham-like energy levels in Fig. 3.

from a spherically averaged density rather than spherically averaging the KSL potential due to the true density. (Cortona[9] makes this same second approximation and claims that it makes no real difference.) Then they calculated the total energy without using these approximations. This is where the problem lies. The KSL potential and the total energy must be calculated using the *same* approximations. The current version of SSCAD calculates the KSL potential and the total energy using the *same* approximations (see Appendix). Thus, the densities obtained from the self-consistent solutions of the KSL equations in SSCAD exactly minimize the energy calculated by SSCAD, as demonstrated in Figs. 3 and 4.

A particular problem arises with the pair approximation when pairs of ions that are quite far apart are included in the calculations. The pair approximation works best near the ions where the electron density is greatest. The greatest error introduced by the pair approximation occurs between the atoms, where three or more ions make major contributions to the total electron density. This error becomes especially large when the contributions from ions very far away are included.

In Fig. 5 we show the relative energy per unit cell in MgO as a function of charge transfer ΔQ from the filled O^{2-} $2p$ orbitals to the empty Mg^{2+} $3s$ orbital. Calculations of the potential about each ion included contributions from hundreds of neighboring ions. The data connected with solid lines were calculated using the pair approximation. The data represented by open circles were calculated using PIB, and the data represented by filled circles were calculated using SSCAD. PIB predicts a charge transfer of about 0.08, and SSCAD predicts a charge transfer of about 0.01. We would expect $Mg^{2+}O^{2-}$ to be very stable against charge transfer, so something is obviously wrong with these calculations. The Mg $3s$ orbital has a long tail which increases the overlap of densities between ions. This problem is not as bad in SSCAD since the increase in the kinetic energy part of the KSL potential due to overlap of densities between ions tends to shorten the length of this tail.

The data connected with dashed lines in the figure were calculated with the correction due to many-body interactions included. As can be seen, both SSCAD and PIB give similar results and predict the expected stability of $Mg^{2+}O^{2-}$ against charge transfer. In PIB, the correction is only made in the energy calculation. The density calculation is not affected. The Mg $3s$ orbital still has the same long tail. In SSCAD, the correction is also included in the calculation of the KSL potential so that the long tails are inhibited. Apparently, when many-body interactions are included in the energy calculation, the presence of long tails in the ion densities does not significantly lower or raise the total energy.

In Fig. 6 we show how the number N of neighbors affects the calculations. We plot the difference ΔE between the KSL energy of the Mg $3s$ orbital and the KSL energy of the O $2p$ orbitals. In this calculation, the Mg $3s$ orbital is empty and the O $2p$ orbitals are full. When ΔE is negative, the KSL energy of Mg $3s$ orbital is lower than that of the O $2p$ orbitals, and we can lower the total energy of the crystal by transferring charge from the O to the Mg ions. The solid line connects data which were calculated using the pair approximation. The dashed line connects data which were calculated with the correction due to many-body interactions

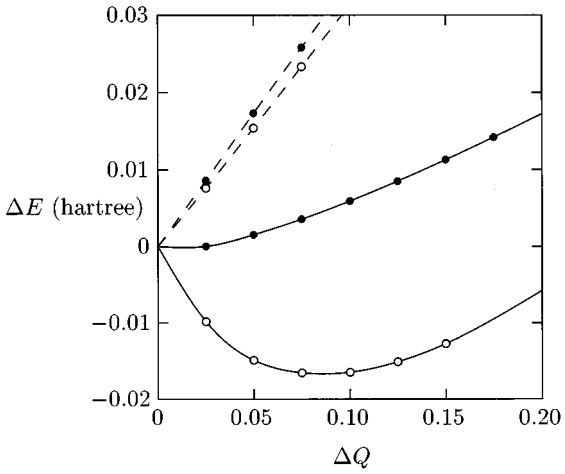

FIG. 5. Relative energy ΔE per unit cell of MgO as a function of charge transfer ΔQ from the O $2p$ orbitals to the Mg $3s$ orbital. The open circles represent calculations made with PIB, and the filled circles represent calculations made with SSCAD. The data connected with solid lines use the pair approximation, and the data connected with dash lines use the correction due to many-body interactions.

included. We see that when 56 or more neighbors are included in the calculation, the pair approximation predicts charge transfer. On the other hand, when we include many-body interactions, the difference in energy is relatively insensitive to the number of neighbors and predicts the expected stability of MgO against charge transfer.

So far in our experience, we have found that the correction for many-body interactions does not significantly affect calculations where only *positions* of ions are varied, such as the determination of crystalline structure and phonon spectra. Thus far, it appears that we only need to include many-body interactions when we are considering charge transfer between ions.

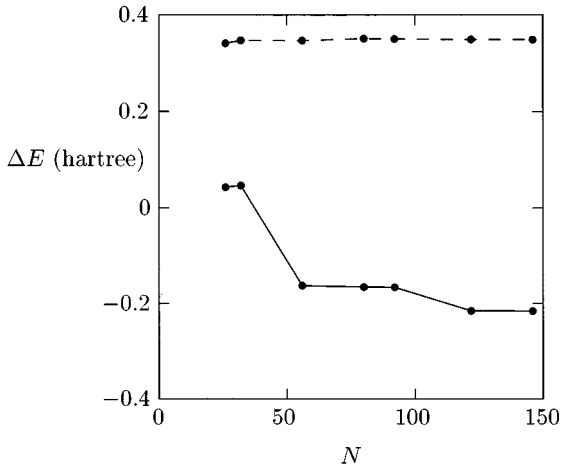

FIG. 6. Difference ΔE between the Kohn-Sham-like energy levels of the Mg $3s$ and O $2p$ orbitals in MgO as a function of the number N of neighboring ions included in the calculation. In these calculations, the Mg $3s$ orbitals are empty, and the O $2p$ orbitals are full. The data connected with solid lines use the pair approximation, and the data connected with dash lines use the correction due to many-body interactions.

ACKNOWLEDGMENTS

This work was supported by the Office of Naval Research. We thank Dr. Mark Pederson, Dr. R. Steven Turley, and Dr. David D. Allred for useful discussions.

APPENDIX: KSL POTENTIAL

We give here details of how we construct the Kohn-Sham-like (KSL) potential used in SSCAD. We write the total energy of the crystal as a functional of the electron density:

$$E=\sum_i T_i+\frac{1}{2}\sum_{\substack{ij\\ i\neq j}}\frac{Z_iZ_j}{|\mathbf{r}_{0i}-\mathbf{r}_{0j}|}-\sum_i\int d^3r\frac{Z_i\rho(\mathbf{r})}{|\mathbf{r}-\mathbf{r}_{0i}|}+\frac{1}{2}\int d^3r\int d^3r'\frac{\rho(\mathbf{r})\rho(\mathbf{r}')}{|\mathbf{r}-\mathbf{r}'|}+\int d^3r\rho(\mathbf{r})\epsilon_{\rm xc}[\rho(\mathbf{r})]+\sum_i\int d^3r\rho_i(\mathbf{r})\{\epsilon_{\rm k}[\rho(\mathbf{r})]-\epsilon_{\rm k}[\rho_i(\mathbf{r})]\},\tag{A1}$$

where T_i is the kinetic energy of the ith ion, Z_i is the charge of the ith nucleus, and $\mathbf{r}_{0i}$ is the position of the ith nucleus. The last term is the correction to the kinetic energy due to overlap of ionic densities. We use the expression of Hedin and Lundqvist[16] for the exchange-correlation energy per electron in a gas of interacting electrons with uniform density:

$$\epsilon_{\rm xc}=-\tfrac{3}{4}(3\rho/\pi)^{1/3}-\tfrac{1}{2}C[(1+z^{-3})\ln(1+z)-z^{2-}+\tfrac{1}{2}z^{-1}-\tfrac{1}{3}],\tag{A2}$$

where

$$z^{-1}=A\left(\frac{3}{4}\pi\rho\right)^{1/3},\tag{A3}$$

and $A=21$ and $C=0.045$. For small values of ρ (less than 10^{-10} when using 8-byte real numbers), Eq. (10) is more accurately evaluated using an expansion in powers of z:

$$\epsilon_{\rm xc}=-\tfrac{3}{4}(3\rho/\pi)^{1/3}-C(\tfrac{3}{4}z-\tfrac{3}{10}z^2+\tfrac{1}{6}z^3-\tfrac{3}{28}z^4+\tfrac{3}{40}z^5).\tag{A4}$$

The kinetic energy per electron in a gas of interacting electrons with uniform density (Thomas-Fermi energy) is given by

$$\epsilon_{\rm k}=\tfrac{3}{10}(3\pi^2\rho)^{2/3}.\tag{A5}$$

From density-functional theory, we obtain a result analogous to that of Kohn and Sham.[14] We obtain for each ion the one-particle Schrödinger-like equation given in Eq. (4), where the KSL potential $\overline{V_i}(r_i)$ is the spherical average of

$$V_i(\mathbf{r})=-\sum_j\frac{Z_j}{|\mathbf{r}-\mathbf{r}_{0j}|}+\sum_j\int d^3r'\frac{\rho_j(\mathbf{r}')}{|\mathbf{r}-\mathbf{r}'|}+V_{\rm xc}[\rho(\mathbf{r})]+V_{\rm k}[\rho(\mathbf{r})]-V_{\rm k}[\rho_i(\mathbf{r})],\tag{A6}$$

where

$$V_{\rm xc}(\rho)=\frac{d}{d\rho}[\rho\epsilon_{\rm xc}(\rho)]=-(3\rho/\pi)^{1/3}-C\ln(1+A\rho^{1/3})\tag{A7}$$

and

$$V_{\rm k}(\rho)=\frac{d}{d\rho}[\rho\epsilon_{\rm k}(\rho)]=\frac{1}{2}(3\pi^2\rho)^{2/3}.\tag{A8}$$

We divide the KSL potential into intraionic and interionic contributions:

$$\overline{V_i}(r_i)=V_i^{\rm intra}(r_i)+\overline{V_i^{\rm inter}}(r_i).\tag{A9}$$

The intraionic contribution consists of a long-range electrostatic potential, a short-range electrostatic potential, and an exchange-correlation KSL potential:

$$V_i^{\rm intra}(r_i)=-\frac{Z_i-N_i}{r_i}+V_{{\rm H},i}(r_i)+V_{\rm xc}(\rho_i),\tag{A10}$$

where N_i is the number of electrons in the ith ion. The short-range electrostatic potential (the short-range Hartree potential) is given by

$$V_{{\rm H},i}(r_i)=-\frac{N_i}{r_i}+\int d^3r'\frac{\rho_i(r_i')}{|\mathbf{r}-\mathbf{r}'|}.\tag{A11}$$

This potential goes to zero outside the ionic electron cloud. Evaluating this equation, we obtain

$$V_{{\rm H},i}(r_i)=4\pi\int_{r_i}^{\infty}\rho_i(r_i')r_i'dr_i'-\frac{4\pi}{r_i}\int_{r_i}^{\infty}\rho_i(r_i')(r_i')^2dr_i'.\tag{A12}$$

The interionic contribution to the KSL potential consists of a long-range electrostatic potential, a short-range electrostatic potential, the exchange-correlation KSL potential due to overlap with neighboring ions, and a contribution from kinetic energy due to overlap with neighboring ions:

$$\overline{V_i^{\rm inter}}(r_i)=\overline{V_{M,i}}(r_i)+\sum_{j\neq i}\overline{V_{{\rm H},j}}(r_i)+\overline{V_{\rm xc}^{\rm overlap}}(r_i)+\overline{V_{\rm k}^{\rm overlap}}(r_i).\tag{A13}$$

The bars over the functions denote a spherical average about $\mathbf{r}_{0i}$ which is the origin of the coordinate system we are using.

The long-range electrostatic potential is the Madelung potential,

$$V_{M,i}(\mathbf{r})=-\sum_{\substack{j\\ j\neq i}}\frac{Z_j-N_j}{|\mathbf{r}-\mathbf{r}_{0j}|}.\tag{A14}$$

Its spherical average about $\mathbf{r}_{0i}$ is given by

$$\overline{V_{M,i}}(r_i)=V_{M,i}(0)+\sum_{\substack{j\\ j\neq i\\ r_i>d_{ij}}}(Z_j-N_j)\left(\frac{1}{d_{ij}}-\frac{1}{r_i}\right),\tag{A15}$$

where d_{ij} is the distance between the nuclei of the ith and jth ions and $V_{M,i}(0)$ is the Madelung potential at the nucleus of the ith ion and is evaluated using the Ewald method.[25]

The short-range electrostatic potential is the short-range Hartree potential due to the the electron cloud of the jth ion. The form is the same as Eq. (20), except that now the result is spherically symmetric about $\mathbf{r}_{0j}$:

$$V_{\mathrm{H},j}(r_j)=4\pi\int_{r_j}^{\infty}\rho_j(r_j')r_j'dr_j'-\frac{4\pi}{r_j}\int_{r_j}^{\infty}\rho_j(r_j')(r_j')^2dr_j'. \tag{A16}$$

We spherically average this potential about $\mathbf{r}_{0i}$, using a method from Lowdin:[26]

$$\overline{V_{\mathrm{H},j}}(r_i)=\frac{1}{2r_id_{ij}}\int_{|r_i-d_{ij}|}^{r_i+d_{ij}}V_{\mathrm{H},j}(r_j)r_jdr_j. \tag{A17}$$

The exchange-correlation KSL potential due to overlap with neighboring ions is divided into two parts:

$$V_{\mathrm{xc}}^{\mathrm{overlap}}(\mathbf{r})=\sum_{\substack{j\\ j\neq i}}V_{\mathrm{xc}}^{\mathrm{pair}}(\rho_i,\rho_j)+V_{\mathrm{xc}}^{\mathrm{many\text{-}body}}(\mathbf{r}). \tag{A18}$$

The first term is due to overlap between *pairs* of ions, and the second term is the correction due to many-body interactions. As we will see below, the first term can be spherically averaged with integrations over a single variable. The second term must be spherically averaged with an integration over two variables on the surface of a sphere. With the contribution due to pair interactions removed, this term is slowly varying in $\mathbf{r}$, allowing us to do the integration with sufficient accuracy. The KSL potential due to overlap between a single pair of ions is given by

$$V_{\mathrm{xc}}^{\mathrm{pair}}(\rho_i,\rho_j)=V_{\mathrm{xc}}(\rho_i+\rho_j)-V_{\mathrm{xc}}(\rho_i). \tag{A19}$$

This potential has a sharp peak at $\mathbf{r}_{0j}$ and is difficult to spherically average about $\mathbf{r}_{0i}$. We overcome this difficulty by dividing the potential into two parts:

$$V_{\mathrm{xc}}^{\mathrm{pair}}(\rho_i,\rho_j)=[V_{\mathrm{xc}}(\rho_j)]+[V_{\mathrm{xc}}(\rho_i+\rho_j)-V_{\mathrm{xc}}(\rho_i)-V_{\mathrm{xc}}(\rho_j)]. \tag{A20}$$

The first part is spherically symmetric about $\mathbf{r}_{0j}$ and can be spherically averaged about $\mathbf{r}_{0i}$ using the method of Lowdin, as in Eq. (25). The second part has the peak at $\mathbf{r}_{0j}$ removed. We obtain

$$\overline{V_{\mathrm{xc}}^{\mathrm{pair}}}(\rho_i,\rho_j)=\frac{1}{2r_id_{ij}}\int_{|r_i-d_{ij}|}^{r_i+d_{ij}}V_{\mathrm{xc}}(\rho_j)r_jdr_j+\frac{1}{2}\int_{-1}^{1}dx[V_{\mathrm{xc}}(\rho_i+\rho_j)-V_{\mathrm{xc}}(\rho_i)-V_{\mathrm{xc}}(\rho_j)], \tag{A21}$$

where x is the cosine of the angle between $\mathbf{r}_{0j}-\mathbf{r}_{0i}$ and $\mathbf{r}-\mathbf{r}_{0i}$. The variable x is hidden in the argument of ρ_j which is $r_j=(r_i^2+d_{ij}^2-2r_id_{ij}x)^{1/2}$. The correction due to many-body interactions is given by

$$\overline{V_{\mathrm{xc}}^{\mathrm{many\text{-}body}}}(\rho_i)=\frac{1}{4\pi}\int d\Omega_i\left\{V_{\mathrm{xc}}(\rho)-V_{\mathrm{xc}}(\rho_i)-\sum_{\substack{j\\ j\neq i}}[V_{\mathrm{xc}}(\rho_i+\rho_j)-V_{\mathrm{xc}}(\rho_i)]\right\}, \tag{A22}$$

where the integration is a spherical average centered at the ith ion. This two-dimensional integration requires a large fraction of the total time required to calculate the KSL potential. In the ''pair approximation'' used in GK, this term is omitted.

The contribution to the KSL potential from kinetic energy due to overlap with the jth ion is given by the same expressions as Eqs. (A18)–(A22), changing the subscripts xc to k.

After obtaining the electron wave functions and densities self-consistently, we can easily calculate the total energy:

$$E=\sum_i T_i+E_M+\sum_i\int d^3r\rho_i\overline{E_i}(r_i). \tag{A23}$$

The first term is the intraionic kinetic energy:

$$T_i=-\frac{1}{2}\sum_{n,l}N_{inl}\int d^3r\psi_{inlm}(\mathbf{r})\nabla^2\psi_{inlm}(\mathbf{r}). \tag{A24}$$

The second term is the total Madelung energy due to point charges at the ions:

$$E_M=\frac{1}{2}\sum_{i,j}\frac{(Z_i-N_i)(Z_j-N_j)}{d_{ij}}. \tag{A25}$$

In the third term, the potential $\overline{E_i}(r_i)$ is the same as the KSL potential $V_i(r_i)$ for the ith ion with the following changes: $V_{\mathrm{xc}}\rightarrow\epsilon_{\mathrm{xc}}$, $V_{\mathrm{k}}\rightarrow\epsilon_{\mathrm{k}}$, $V_{\mathrm{H},i}\rightarrow\frac{1}{2}V_{\mathrm{H},i}$, and

$$\overline{V_{M,i}}(r_i)\rightarrow\sum_{\substack{j\\ j\neq i\\ r_i>d_{ij}}}\left(Z_j-\frac{1}{2}N_j\right)\left(\frac{1}{d_{ij}}-\frac{1}{r_i}\right). \tag{A26}$$

The factor $\frac{1}{2}$ in the above changes compensates for the double counting which results when i and j are interchanged.

In the PIB model, the interionic contribution to the KSL potential is simply given by

$$\overline{V_i^{\mathrm{inter}}}(r_i)=\begin{cases}V_{M,i}(0), & r_i<r_w\\ (r_w/r_i)V_{M,i}(0), & r_i>r_w,\end{cases} \tag{A27}$$

where r_w is the radius of the Watson sphere, given by

$$r_w=\frac{Z_i-N_i}{V_{M,i}(0)}. \tag{A28}$$

The total energy is calculated in PIB exactly the same as in SSCAD.

*Present address: Department of Physics and Astronomy, Brigham Young University, Provo, Utah 84602.

[1] R. G. Gordon and Y. S. Kim, J. Chem. Phys. **56**, 3122 (1972).
[2] R. G. Gordon and R. LeSar, Adv. Quantum Chem. **21**, 341 (1990).
[3] C. Muhlhausen and R. G. Gordon, Phys. Rev. B **23**, 900 (1981).
[4] R. E. Watson, Phys. Rev. **111**, 1108 (1958).
[5] L. L. Boyer, M. J. Mehl, J. L. Feldman, J. R. Hardy, J. W. Flocken, and C. Y. Fong, Phys. Rev. Lett. **54**, 1940 (1985); **57**, 2331 (1986).
[6] M. J. Mehl, R. J. Hemley, and L. L. Boyer, Phys. Rev. B **33**, 8685 (1986).
[7] R. E. Cohen, L. L. Boyer, and M. J. Mehl, Phys. Rev. B **35**, 5749 (1987).
[8] P. J. Edwardson, Phys. Rev. Lett. **63**, 55 (1989).
[9] P. Cortona, Phys. Rev. B **44**, 8454 (1991).
[10] P. Cortona, Phys. Rev. B **46**, 2008 (1992).
[11] L. L. Boyer and M. J. Mehl, Ferroelectrics **150**, 13 (1993).
[12] L. L. Boyer, H. T. Stokes, and M. J. Mehl, Ferroelectrics **164**, 177 (1995).
[13] M. J. Mehl, L. L. Boyer, and H. T. Stokes, J. Phys. Chem. Solids (to be published).
[14] W. Kohn and L. J. Sham, Phys. Rev. **140**, A1133 (1965).
[15] P. D. Tepesch, A. F. Kohan, G. D. Garbulsky, G. Ceder, C. Coley, H. T. Stokes, L. L. Boyer, M. J. Mehl, B. P. Burton, K. Cho, and J. Joannopoulos, J. Am. Ceramic Soc. **79**, 2033 (1996).
[16] L. Hedin and B. I. Lundqvist, J. Phys. C **4**, 2064 (1971).
[17] E. Clementi and C. Roetti, At. Data Nucl. Data Tables **14**, 177 (1974).
[18] A. D. McLean and R. S. McLean, At. Data Nucl. Data Tables **26**, 197 (1981).
[19] G. H. Wolf and M. S. T. Bukowinski, Phys. Chem. Min. **15**, 209 (1988).
[20] M. J. L. Sangster, G Peckham, and D. H. Saunderson, J. Phys. C **3**, 1026 (1970).
[21] C. Kittel, *Introduction to Solid State Physics*, 4th ed. (Wiley, New York, 1971).
[22] I. Jackson and H. Niesler, in *High-Pressure Research in Geophysics*, edited by S. Akimoto and M. H. Manghnani (Reidel, Dordrecht, 1982), p. 93.
[23] M. J. Mehl, B. M. Klein, and D. A. Papaconstantopoulos, in *Intermetallic Compounds. Vol. 1: Principles*, edited by J. A. Westbrook and R. L. Fleischer (John Wiley, London, 1994), Chap. 9.
[24] J. F. Janak, Phys. Rev. B **18**, 7165 (1978).
[25] J. C. Slater, *Quantum Theory of Molecules and Solids* (McGraw-Hill, New York, 1967), Vol. 3, pp. 215–220.
[26] P. O. Lowdin, Adv. Phys. **5**, 1 (1956).